Electronic Supplementary Material (ESI) for Journal of Materials Chemistry A.

Supporting Information

Freestanding Ultralight Metallic Micromesh for High–energy Density Flexible Transparent Supercapacitors

*Guanhua Zhang[a,b], Yanli Zhao[a], Jin Hu[a], Huaizhi Liu[a], Tianwei Chen[a], Huihuang Yu[a], and Huigao Duan[a,b]**

[a] State Key Laboratory of Advanced Design and Manufacturing for Vehicle Body College of Mechanical and Vehicle Engineering, Hunan University, Changsha, 410082, PR. China.

[b] Greater Bay Area Institute for Innovation, Hunan University, Guangzhou 511300, Guangdong Province, China

Correspondence should be addressed to Huigao Duan; duanhg@hnu.edu.cn

Section 1. Calculation method:

The areal capacitance C_s and C_g were calculated from the GCD curves through the following equations:

$$C_s = \frac{I \times \Delta t}{S \times 3600} \quad (1)$$

$$C_g = \frac{I \times \Delta t}{m \times \Delta V} \quad (2)$$

Where C_s (mAh cm^{-2}) and C_g (F g^{-1}) are the specific capacitance, S (cm^2) is the geometric area of the electrodes, I (mA cm^{-2}) is the charge/discharge current density, and Δt (s) is the discharge time, ΔV (V) is the potential window and m (mg) is the loading mass of the active material. The energy density (E, W h cm^{-2}) and power density (P, W cm^{-2}) were calculated by equation (3) and (4) as follows:

$$E = \frac{C_S \times \Delta V^2}{2} \quad (3)$$

$$P = \frac{E}{\Delta t} \quad (4)$$

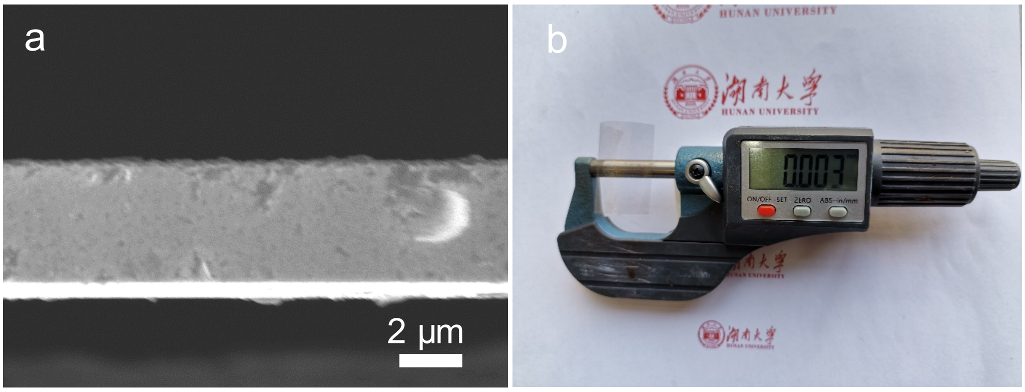

Fig 1. (a) SEM image of cross–sectional of NM. (b) Micrometer for measuring the cross–sectional thickness of NM.

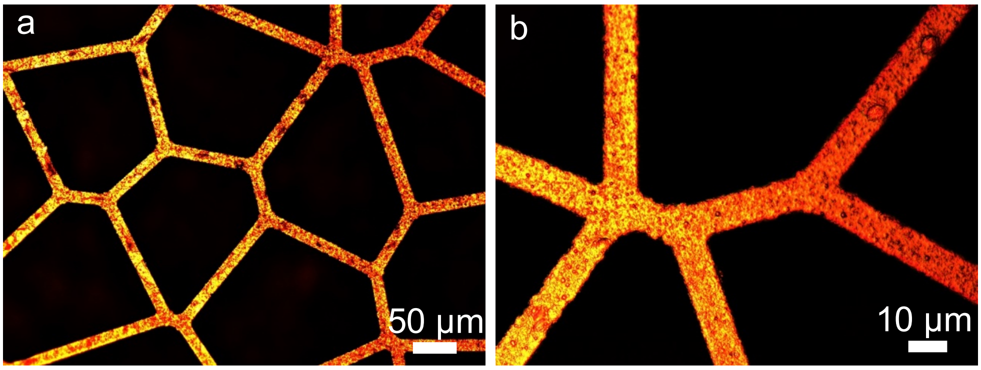

Fig 2. Optical microscope image of NM@NiCoP.

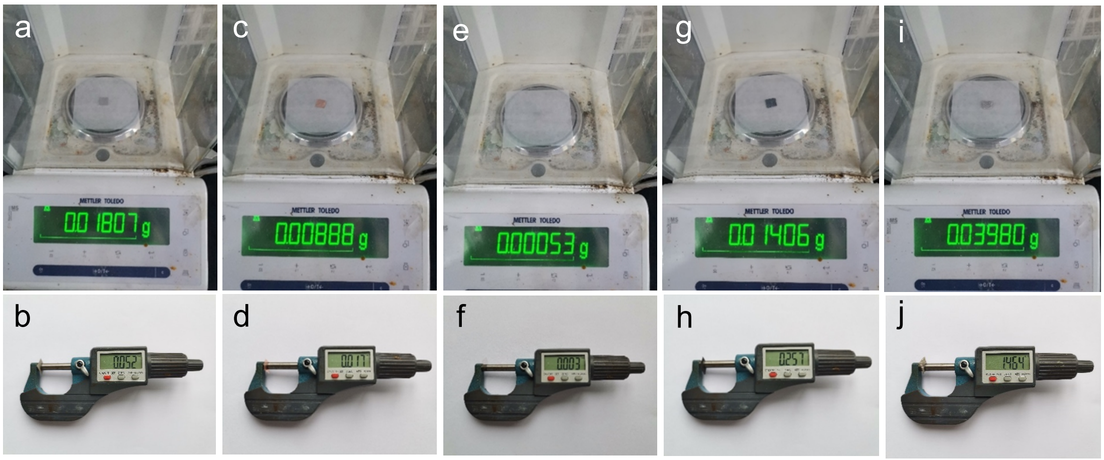

Fig 3. Weight (a,c,e,g,i) and thickness measurement (b,d,f.h.j) of 1×1cm^2 stainless steel mesh (SSN), copper foil (CF), nickel mesh (NM), carbon cloth (CC) and nickel foam (NF), respectively.

Fig 4. The crimping process of transparent NM on a glass rod.

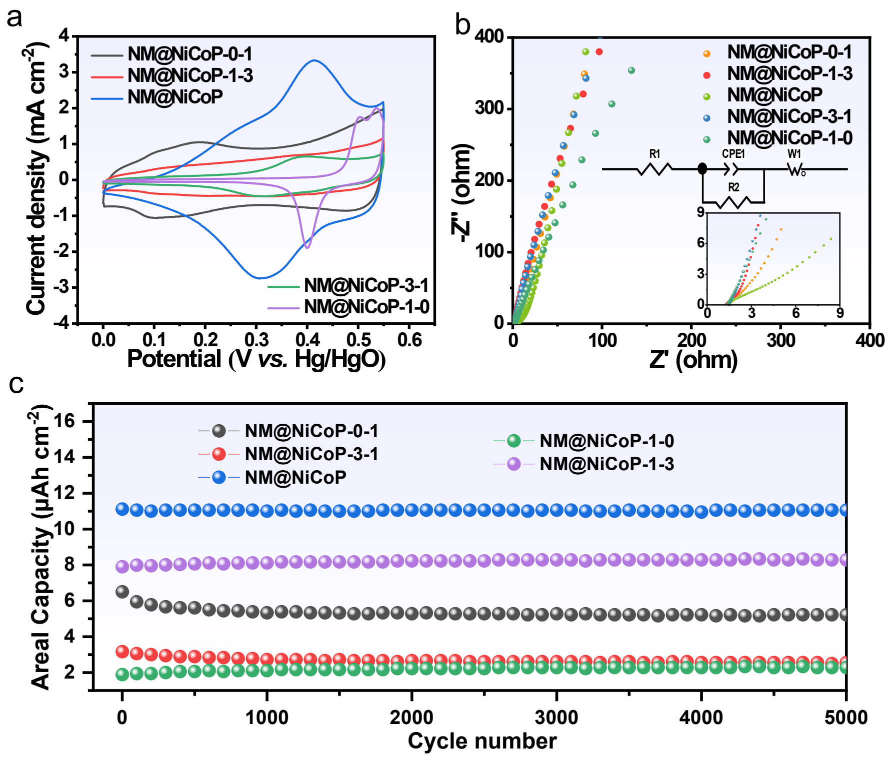

Fig 5. (a) CV curves of NM@NiCoP–*x*–*y* in the voltage range of 0–0.55 V at a scan rate of 20 mV s^{-1}. (b) Electrochemical impedance spectroscopy (EIS) of NM@NiCoP–*x*–*y* in the frequency range of 100 kHz to 0.01 Hz. (c) Cycling stability of NM@NiCoP–*x*–*y* at a current density of 2 mA cm^{-2}.

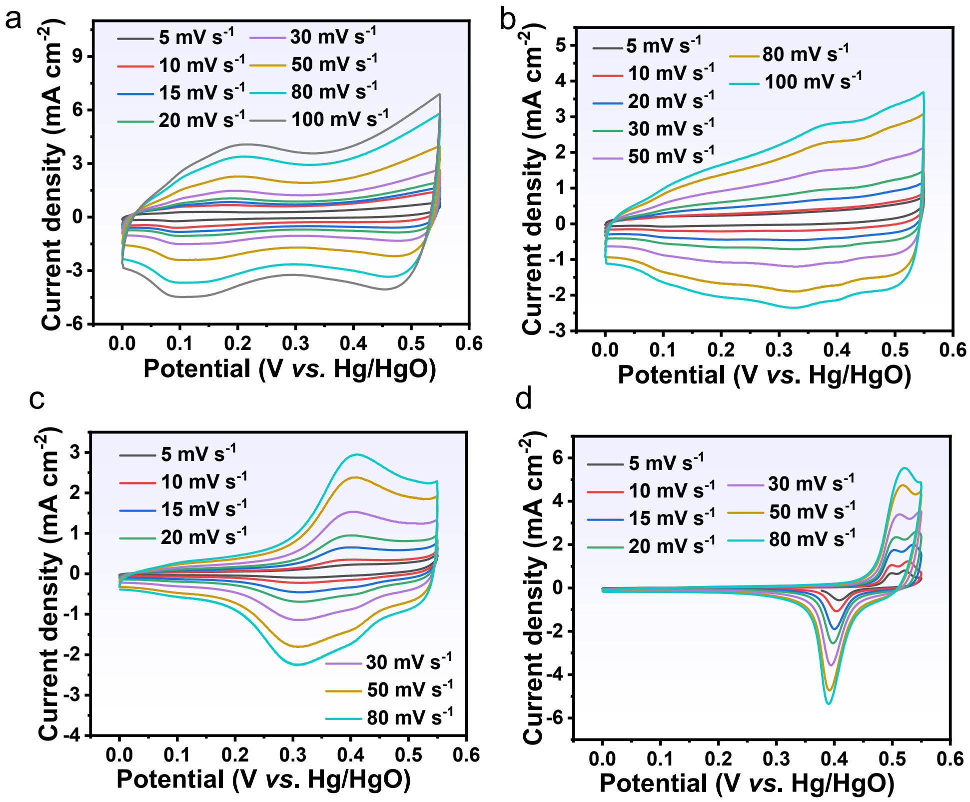

Fig 6. The respective CV curves of (a) NM@NiCoP–0–1, (b) NM@NiCoP–1–3, (c) NM@NiCoP–3–1 and (d) NM@NiCoP–1–0 at different scan rates.

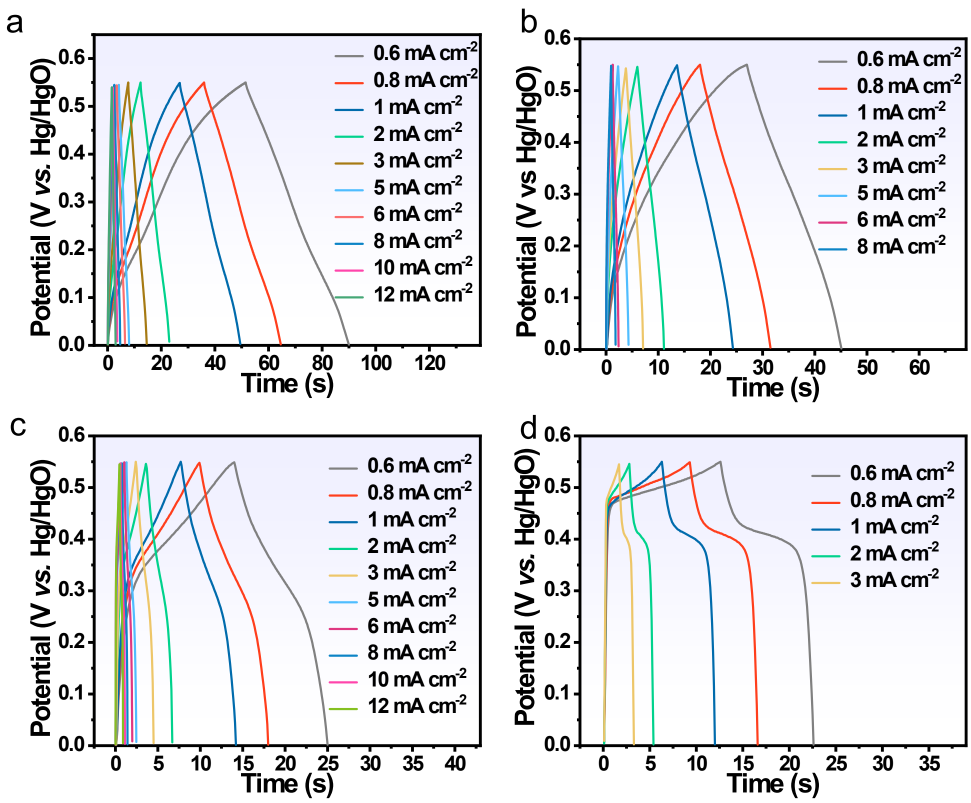

Fig 7. GCD curves of (a) NM@NiCoP–0–1, (b) NM@NiCoP–1–3, (c) NM@NiCoP–3–1 and (d) NM@NiCoP–1–0 at various current densities.

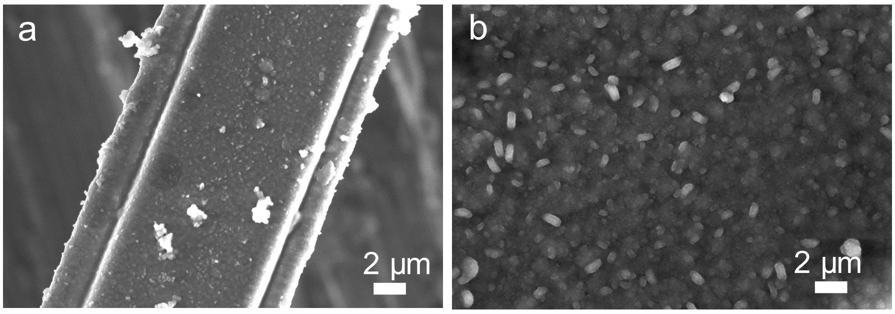

Fig 8. SEM images of NM@NiCoP electrode after 20,000 GCD cycles.

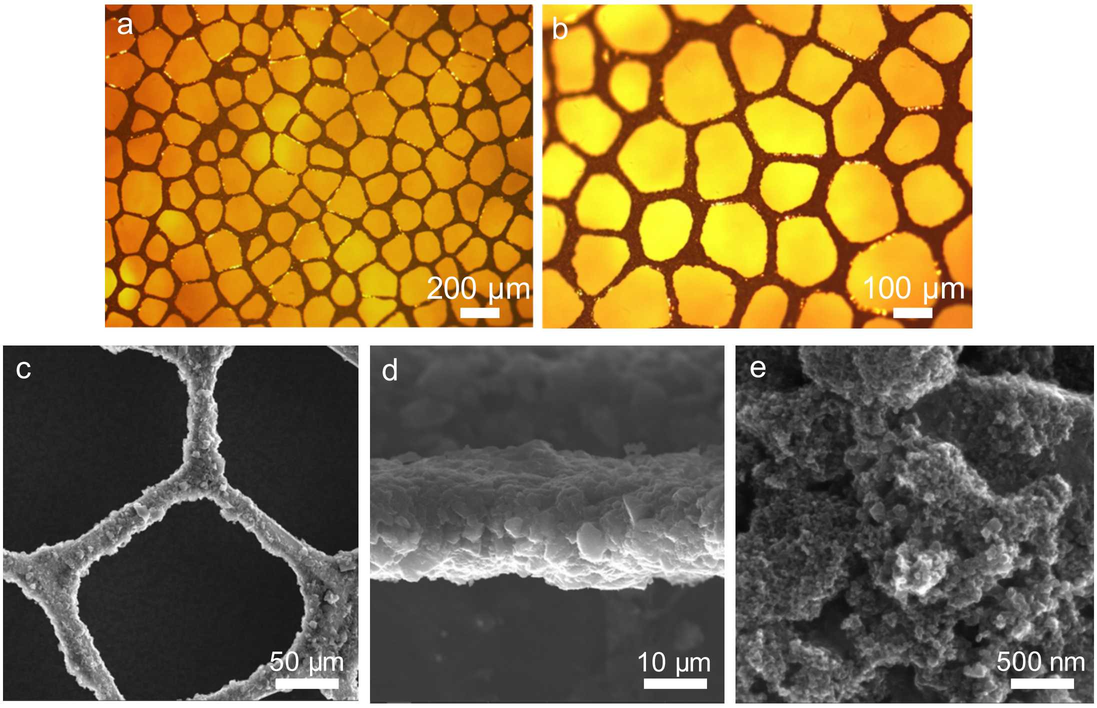

Fig 9 (a,b) Optical microscope image of NM@NPC electrode. (c) SEM image of NM@NPC electrode. (d) SEM image of the cross–sectional thickness of the NM@NPC electrode. (e) Magnified SEM image of NPC active material.

Fig 10. Electrochemical performance of the NM@NPC. (a) CV curves, (b) GCD curves and (c) Nyquist impedance spectra of the NM@NPC. (d) Rate performance and (e) Capacity retention for 10,000 cycles of the NM@NPC.

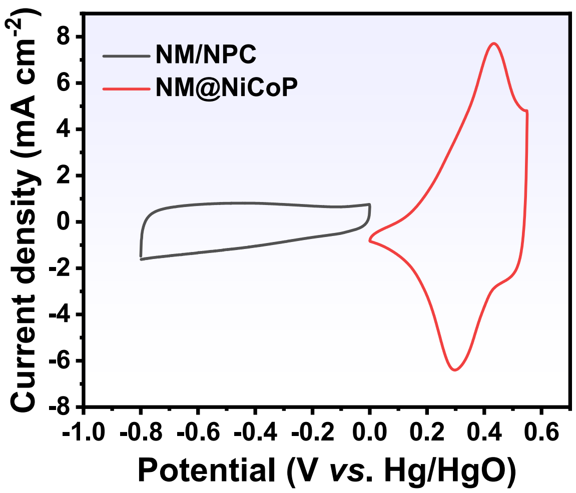

Fig 11. CV plots of the NPC anode and NM@NiCoP cathode performed in 2 M KOH at 50 mV s^{-1}.

Fig 12. (a) CV curves obtained at different scanning rates from 5 to 100 mV s^{-1}. (b) GCD curves of at various current densities from 1 to 12 mA cm^{-2}. (c) The Nyquist impedance spectra of the aqueous electrolyte device. (d) Rate capability of the device at various current rates. (e) Cycling performance of the device at a current density of 2 mA cm^{-2}.

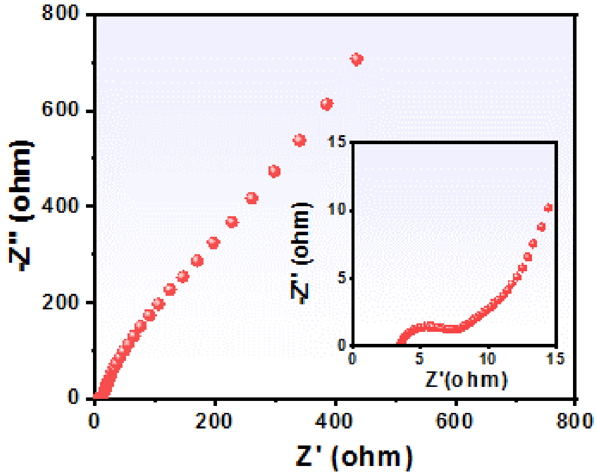

Fig 13. The Nyquist impedance spectra of the NM@NiCoP//PVA/KOH//NM@NPC device.

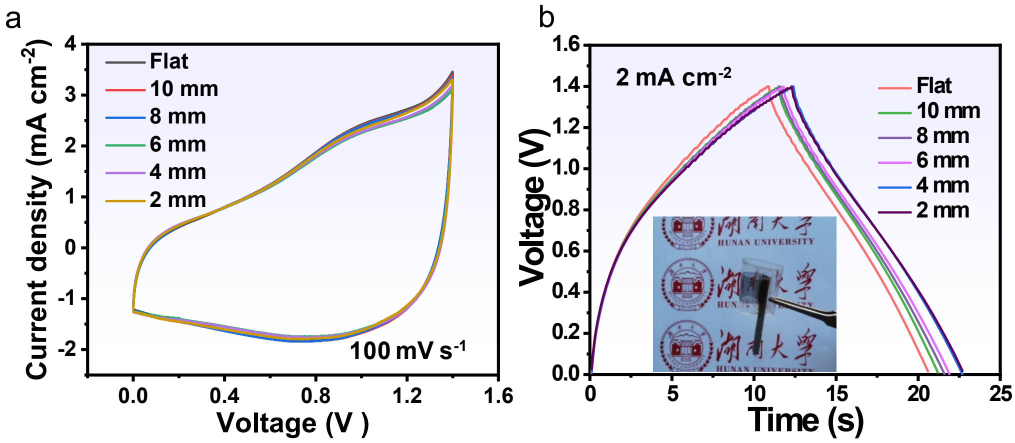

Fig 14. (a) CV curves of the all–solid–state device being bent from the flat to the radius of curvature of 2 mm. (b) GCD curves of the device being bent from the flat to the radius of curvature of 2 mm (Insert image: optical photo of the device being bent).

Table S1. Performance comparison of flexible transparent energy supercapacitors

Electrode material	T_E(%) (550nm)	T_D(%) (550nm)	Gel electrolyte	Device type	Voltage window(V)	Cycle performance	Areal capacity	Energy density	Power density	Ref.
NM@NiCoP//NM@NPC	**80.2**	**67.5**	**PVA/KOH**	**√**	**1.4**	**50000, 97.6% (10 mA cm^{-2})**	**21.1 mF cm^{-2} 8.2 µAh cm^{-2} (0.6 mA cm^{-2})**	**8.0 µWh cm^{-2}**	**980 µW cm^{-2}**	**This work**
MnO_2–Au–Ni//MnO_2–Au–Ni	73	62	PVA/LiCl	×	0.8	/	34.8 mF cm^{-2} (0.01V s^{-1})	/	/	[1]
Au@MnO_2//Au@MnO_2	60	36	$LiClO_4$/PVA	×	1.0	/	795 µF cm^{-2} (5 µA cm^{-2})	/	/	[2]
2L Gr//2L Gr	78.7	75	PVA/H_2SO_4	×	0.8	/	99.4 mF cm^{-2} (1.8 µA cm^{-2})	/	/	[3]
Au/GP//Au/GP	69.3	59	PVA/H_2SO_4	×	1.0	20000, 95.4% (0.3 mA cm^{-2})	3.3 mF cm^{-2}	430 µWh cm^{-3}	190 mW cm^{-3}	[4]
PEDOT:PSS//PEDOT:PSS	78	55-67	H_3PO_4/PVA	×	0.8	1000, 100% (0.01 mA cm^{-2})	4.72 mFcm^{-2}	0.074 mW h cm^{-2}	0.036 W cm^{-2}	[5]
MnO_2@Ni//MnO_2@Ni	83.91	80.82	PVA/LiCl	×	0.8	10000, 100% (20 V s^{-1})	10.6 mF cm^{-2} (10 mV s^{-1})	/	/	[6]
Gr@Ag//Gr@Ag	74	65	PVA/H_3PO_4	×	1.0	10000, 100% (0.024 mA cm^{-2})	0.3 mF cm^{-2} (0.1 V s^{-1})	9.7 nWh cm^{-2}	2.5 µW cm^{-2}	[7]
PPy/AuLV//PPy/AuLV	65	45	PVA/LiCl	×	0.6	2500, 83% (1mA cm^{-2})	5.6 mF cm^{-2} (1 mA cm^{-2})	0.28 µWh cm^{-2}	80 µW cm^{-2}	[8]
AgNW/PEDOT:PSS// AgNW/PEDOT:PSS	80	/	H_3PO_4/PVA	×	1.0	2500, 90% (0.25 mA cm^{-2})	8.58 mF cm^{-2} (0.1 mA cm^{-2})	/	/	[9]

AgNW@NiCo/NiCo(OH)$_2$// Ag NW/graphene	54	36	PVA/LiClO$_4$/ KOH	√	0.7	5000, 91.9% (100 mV s^{-1})	9.6 mF cm^{-2} (0.2 mA cm^{-2})	3.0 W h kg^{-1}	3.5 W kg^{-1}	[10]
MnO$_2$@Au−Ni// MnO$_2$@Au−Ni	69.4	60	PVA/LiCl	×	0.8	10000, 96.5% (100V s^{-1})	78.46 mF cm^{-2} (100 Vs^{-1})	/	/	[11]
LSMCS//LSMCS	85–88	80	PVA/H$_3$PO$_4$	×	1.6	5000, 57.9% 10 mV s^{-1}	0.19 mF cm^{-2} (10 mV s^{-1})	0.068 µWh cm^{-2}	47.08 µWcm^{-2}	[12]
Co(OH)$_2$/AgNW// Co(OH)$_2$/AgNW	90	54	PVA/KCl	×	0.6	10000, 91%	540 µC cm^{-2} (10mV s^{-1})	0.04 µWh cm^{-2}	28.8 mW cm^{-2}	[13]
PEDOT:PSS/AgNFs// PEDOT:PSS/AgNFs	84.7	77	H$_2$SO$_4$/PVA	×	1.0	10000, 95% (37 µA cm^{-2})	0.91 mF cm^{-2} (5 mV s^{-1})	0.09 µWh cm^{-2}	0.93 µW cm^{-2}	[14]
MnO$_2$@AuNFs// MnO$_2$@AuNFs	93.13	79	LiCl/PVA	×	0.8	10000, 94% (75 µA cm^{-2})	2.07 mF cm^{-2} (5 mV s^{-1})	0.14 µWh cm^{-2}	4 µW cm^{-2}	[15]
Co(OH)2@Ni//Co(OH)2@Ni	75	54	PVA/KOH	×	0.6	10000, 90% (0.09 mA cm^{-2})	5.32 mF cm^{-2} (5 mV s^{-1})	0.42 µWh cm^{-2}	8.33 µW cm^{-2}	[16]
SWCNT/ITO//SWCNT/ITO	/	57.4	PVA/LiCl– PS	×	0.8	10000, 95.3% (20 µA cm^{-2})	120.7 µF cm^{-2}	/	/	[17]
MnO$_2$/AuNF//MnO$_2$/AuNF	71	60	LiClO$_4$/PVA	×	1.0	500, 95% (0.06 mA cm^{-2})	3.68 mF cm^{-2}	56 µWh cm^{-2}	0.51 µW cm^{-2}	[18]
Ag/porous carbon// Ag/Ni$_x$Fe$_y$O$_z$@rGO	84.2//86.3	70.6	PVDF-HFP/ LiTFSI	√	2.5	1000, 88.2% (60 µA cm^{-2})	226.8 µF cm^{-2} (3 µA cm^{-2})	2.7 mWh L^{-1}	1002.5 mW L^{-1}	[19]
Cu@Ni@NiCoS NF// Cu@Ni@NiCoS NF	89	65	PVA/KOH	×	0.6	10000, 89% (0.6 mA cm^{-2})	1.21µAh cm^{-2} (0.025 mA cm^{-2})	0.48 µWh cm^{-2}	11.15 µW cm^{-2}	[20]

PEDOT:PSS// PEDOT:PSS	60	/	PVA/H_3PO_4	×	1.0	3000, 96.8% (0.2 mA cm^{-2})	1.32 mF cm^{-2} (0.1 mA cm^{-2})	0.183 μWh cm^{-2}	4.98 μW cm^{-2}	[21]
Ni@MnO_2//Ni@MnO_2	80	77	PVA/LiCl	×	0.8	10000, 98.6% (10 V s^{-1})	19.65 mF cm^{-2}	/	/	[22]
AgNFs/MoO_3/PEDOT:PSS// AgNFs/MoO_3/PEDOT:PSS	82.8	64.5	PVA/LiCl	×	0.8	15000,.86.6% (0.2 mA cm^{-2})	7.0 mF cm^{-2} (0.1 mA cm^{-2})	0.623 mWh cm^{-2}	40 mW cm^{-2}	[23]
MoS_2/AIP//MoS_2/AIP	79.56	/	PVA/KOH	×	1.0	/	207 mF cm^{-2} (6 mA cm^{-2})	28.78 μWh cm^{-2}	1.03 mW cm^{-2}	[24]
PEDOT//AgNWs/NaxWO_3/ PEDOT	/	55	PVA/H_2SO_4	√	1.2	2000, 80% (0.15 mA cm^{-2})	0.332 mF cm^{-2} (0.05 mA cm^{-2})	2.03–0.72 Wh m^{-2}	393–1299 W m^{-2}	[25]
TSBL–MQD/LRGO	91.14	80	PVA/H_2SO_4	×	1.2	12000, 97.6% (0.9 mA cm^{-2})	10.42 mF cm^{-2}	40.8 Wh kg^{-1}	2513.7 W kg^{-1}	[26]

Note: T_E stands for the optical transmittance of the electrode, and T_D represents the optical transmittance of the device; "√"indicates that the device is an asymmetric device, and "×" indicates that the device is a symmetric device.

Reference

[1] Y. Zhao, Z. Jiang, Y. Weng, Y.-H. Liu, Transparent, stretchable and high-performance supercapacitors based on freestanding Ni-mesh electrode, IOP Conference Series: Earth and Environmental Science 675(1) (2021) 012105, https://doi.org/10.1088/1755-1315/675/1/012105.

[2] T. Qiu, B. Luo, M. Giersig, E.M. Akinoglu, L. Hao, X. Wang, L. Shi, M. Jin, L. Zhi, Au@MnO_2 Core–Shell Nanomesh Electrodes for Transparent Flexible Supercapacitors, Small 10(20) (2014) 4136-4141, https://doi.org/10.1002/smll.201401250.

[3] K. Jo, S. Lee, S.-M. Kim, J.B. In, S.-M. Lee, J.-H. Kim, H.-J. Lee, K.-S. Kim, Stacked Bilayer Graphene and Redox-Active Interlayer for Transparent and Flexible High-Performance Supercapacitors, Chem. Mater. 27(10) (2015) 3621-3627, https://doi.org/10.1021/cm504801r.

[4] N. Li, G. Yang, Y. Sun, H. Song, H. Cui, G. Yang, C. Wang, Free-Standing and Transparent Graphene Membrane of Polyhedron Box-Shaped Basic Building Units Directly Grown Using a NaCl Template for Flexible Transparent and Stretchable Solid-State Supercapacitors, Nano Lett. 15(5) (2015) 3195-3203, https://doi.org/10.1021/acs.nanolett.5b00364.

[5] T. Cheng, Y.-Z. Zhang, J.-D. Zhang, W.-Y. Lai, W. Huang, High-performance free-standing PEDOT:PSS electrodes for flexible and transparent all-solid-state supercapacitors, Journal of Materials Chemistry A 4(27) (2016) 10493-10499, https://doi.org/10.1039/C6TA03537J.

[6] Y.-H. Liu, J.-L. Xu, X. Gao, Y.-L. Sun, J.-J. Lv, S. Shen, L.-S. Chen, S.-D. Wang, Freestanding transparent metallic network based ultrathin, foldable and designable supercapacitors, Energy & Environmental Science 10(12) (2017) 2534-2543, https://doi.org/10.1039/C7EE02390A.

[7] Y. Zhong, X. Zhang, Y. He, H. Peng, G. Wang, G. Xin, Simultaneously Armored and Active Graphene for Transparent and Flexible Supercapacitors, Adv. Funct. Mater. 28(28) (2018) 1801998, https://doi.org/10.1002/adfm.201801998.

[8] S. Chen, B. Shi, W. He, X. Wu, X. Zhang, Y. Zhu, S. He, H. Peng, Y. Jiang, X. Gao, Z. Fan, G. Zhou, J.-M. Liu, K. Kempa, J. Gao, Quasifractal Networks as Current Collectors for Transparent Flexible Supercapacitors, Adv. Funct. Mater. 29(48) (2019) 1906618, https://doi.org/10.1002/adfm.201906618.

[9] D. Li, X. Liu, X. Chen, W.-Y. Lai, W. Huang, A Simple Strategy towards Highly Conductive Silver-Nanowire Inks for Screen-Printed Flexible Transparent Conductive Films and Wearable Energy-Storage Devices, Advanced Materials Technologies 4(8) (2019) 1900196, https://doi.org/10.1002/admt.201900196.

[10] J. Liu, G. Shen, S. Zhao, X. He, C. Zhang, T. Jiang, J. Jiang, B. Chen, A one-dimensional Ag NW@NiCo/NiCo$(OH)_2$ core–shell nanostructured electrode for a flexible and transparent asymmetric supercapacitor, Journal of Materials Chemistry A 7(14) (2019) 8184-8193, https://doi.org/10.1039/C9TA01303B.

[11] Y.-H. Liu, Z.-Y. Jiang, J.-L. Xu, Self-Standing Metallic Mesh with MnO_2 Multiscale Microstructures for High-Capacity Flexible Transparent Energy Storage, ACS Applied Materials & Interfaces 11(27) (2019) 24047-24056, https://doi.org/10.1021/acsami.9b05033.

[12] D.D. Nguyen, C.-H. Hsiao, T.-Y. Su, P.-Y. Hsieh, Y.-L. Chen, Y.-L. Chueh, C.-Y. Lee, N.-H. Tai, Bioinspired networks consisting of spongy carbon wrapped by graphene sheath for flexible transparent supercapacitors, Communications Chemistry 2(1) (2019) 137, https://doi.org/10.1038/s42004-019-0238-9.

[13] H. Sheng, X. Zhang, Y. Ma, P. Wang, J. Zhou, Q. Su, W. Lan, E. Xie, C.J. Zhang, Ultrathin, Wrinkled, Vertically Aligned $Co(OH)_2$ Nanosheets/Ag Nanowires Hybrid Network for Flexible Transparent Supercapacitor with High Performance, ACS Applied Materials & Interfaces 11(9) (2019) 8992-9001, https://doi.org/10.1021/acsami.8b18609.

[14] S.B. Singh, T. Kshetri, T.I. Singh, N.H. Kim, J.H. Lee, Embedded PEDOT:PSS/AgNFs network flexible transparent electrode for solid-state supercapacitor, Chem. Eng. J. 359 (2019) 197-207, https://doi.org/10.1016/j.cej.2018.11.160.

[15] S.B. Singh, T.I. Singh, N.H. Kim, J.H. Lee, A core–shell MnO_2@Au nanofiber

network as a high-performance flexible transparent supercapacitor electrode, Journal of Materials Chemistry A 7(17) (2019) 10672-10683, https://doi.org/10.1039/C9TA00778D.

[16] B.S. Soram, J. Dai, T. Kshetri, N.H. Kim, J.H. Lee, Vertically grown and intertwined $Co(OH)_2$ nanosheet@Ni-mesh network for transparent flexible supercapacitor, Chem. Eng. J. 391 (2020) 123540, https://doi.org/10.1016/j.cej.2019.123540.

[17] J. Chen, W. Xiao, T. Hu, P. Chen, T. Lan, P. Li, Y. Li, B. Mi, Y. Ma, Controlling Electrode Spacing by Polystyrene Microsphere Spacers for Highly Stable and Flexible Transparent Supercapacitors, ACS Applied Materials & Interfaces 12(5) (2020) 5885-5891, https://doi.org/10.1021/acsami.9b19878.

[18] Y. Lee, S. Chae, H. Park, J. Kim, S.-H. Jeong, Stretchable and transparent supercapacitors based on extremely long MnO_2/Au nanofiber networks, Chem. Eng. J. 382 (2020) 122798, https://doi.org/10.1016/j.cej.2019.122798.

[19] T. Liu, R. Yan, H. Huang, L. Pan, X. Cao, A. deMello, M. Niederberger, A Micromolding Method for Transparent and Flexible Thin-Film Supercapacitors and Hybrid Supercapacitors, Adv. Funct. Mater. 30(46) (2020) 2004410, https://doi.org/10.1002/adfm.202004410.

[20] B.S. Soram, I.S. Thangjam, J.Y. Dai, T. Kshetri, N.H. Kim, J.H. Lee, Flexible transparent supercapacitor with core-shell Cu@Ni@NiCoS nanofibers network electrode, Chem. Eng. J. 395 (2020) 125019, https://doi.org/10.1016/j.cej.2020.125019.

[21] X. Guan, L. Pan, Z. Fan, Flexible, Transparent and Highly Conductive Polymer Film Electrodes for All-Solid-State Transparent Supercapacitor Applications, Membranes 11(10) (2021), https://doi.org/10.3390/membranes11100788.

[22] Z.-Y. Jiang, Y.-Y. Zhao, W. Huang, J.-L. Xu, L.-S. Chen, Y.-H. Liu, Hierarchically nanobranch structured freestanding metallic mesh electrode for high-performance transparent flexible supercapacitor, J. Alloys Compd. 861 (2021) 158593, https://doi.org/10.1016/j.jallcom.2020.158593.

[23] J. Liang, H. Sheng, Q. Wang, J. Yuan, X. Zhang, Q. Su, E. Xie, W. Lan, C. Zhang,

PEDOT:PSS-glued MoO_3 nanowire network for all-solid-state flexible transparent supercapacitors, Nanoscale Advances 3(12) (2021) 3502-3512, https://doi.org/10.1039/D1NA00121C.

[24] V. Raman, D. Rhee, A.R. Selvaraj, J. Kim, K. Prabakar, J. Kang, H.-K. Kim, High-performance flexible transparent micro-supercapacitors from nanocomposite electrodes encapsulated with solution processed MoS_2 nanosheets, Science and Technology of Advanced Materials 22(1) (2021) 875-884, https://doi.org/10.1080/14686996.2021.1978274.

[25] W.-M. Huang, C.-Y. Hsu, D.-H. Chen, Sodium tungsten oxide nanowires-based all-solid-state flexible transparent supercapacitors with solar thermal enhanced performance, Chem. Eng. J. 431 (2022) 134086, https://doi.org/10.1016/j.cej.2021.134086.

[26] Y. Yuan, L. Jiang, X. Li, P. Zuo, X. Zhang, Y. Lian, Y. Ma, M. Liang, Y. Zhao, L. Qu, Ultrafast Shaped Laser Induced Synthesis of MXene Quantum Dots/Graphene for Transparent Supercapacitors, Adv. Mater. 34(12) (2022) 2110013, https://doi.org/10.1002/adma.202110013.